Sankhla and Kushwaha
J Mater. Sci: Mater Eng. (2024) 19:11
https://doi.org/10.1186/s40712-024-00157-9

Journal of Materials Science: Materials in Engineering

ORIGINAL PAPER

Open Access

Development of an opto-electrochemical sensor for the detection of malathion using manganese metal–organic framework (Mn-MOF)

Lakshya Sankhla[1] and Himmat Singh Kushwaha[2,3*]

Abstract

This paper presents a new method for detecting malathion pesticides using a modified screen-printed electrode (SPE) with a fluorescence quenching technique. The manganese-based MOF was synthesized using the solvothermal method. The synthesized MOFs were characterized by transmission electron microscopy (TEM), x-ray diffraction (XRD), Fourier transform infrared spectroscopy (FT-IR), and Raman spectroscopy. The material's electrocatalytic properties were assessed via electrochemical impedance spectroscopy (EIS) and cyclic voltammetry (CV). Within the concentration range of 0.89 µM to 5.95 µM, the material's response to malathion was analyzed with square wave voltammetry (SWV), giving rise to a detection limit of 39.097 nM. Fluorescence quenching studies have been carried out between 0.039 and 0.56 µM, with a lower detection limit of 62.03 nM. A sensor with good anti-interference properties was tested for selectivity and practicability in detecting malathion in real samples, proving its potential use in this area.

Keywords Square wave voltammetry (SWV), Screen-printed electrode, Fluorescence quenching, Organophosphate pesticide, Malathion, Mn metal–organic framework

Introduction

An acetylcholinesterase inhibitor, malathion is an organophosphate pesticide. It forms a long-lasting bond upon absorption into the target organism, and the cholinesterase enzyme contains the serine residue (Bonner et al. 2007). Acetylcholine builds up at the synapses fast because of the phosphor-ester group that results from the reaction. It is firmly coupled to cholinesterase and irreversibly inactivates it. With a melting point of 37.1 °F and a boiling temperature of 156–157 °C, it has a skunk-like stench ("Malathion _ C10H19O6PS2 _ CID 4004 - PubChem" n.d.).

According to certain studies, its remnants have been found in food and water sources (Silva-Madera, et al. 2021). As a result, malathion is a major ecological pollutant, and effective environmental monitoring and mitigation are needed to develop low-cost, dependable, and decentralized analytical techniques. Traditional techniques for determining malathion include high-performance liquid chromatography (HPLC) (Huang et al. 2019) and gas chromatography coupled to mass spectrometry (GC–MC) (Xiao et al. 2013). Although these approaches are trustworthy, they need complex sample derivatization, expensive equipment, and highly skilled analysts. Electrochemical methods have recently emerged as a viable choice for toxicant detection due to

*Correspondence:
Himmat Singh Kushwaha
himmat1.singh@mygyanvihar.com; himmatsingh.mrc@mnit.ac.in
[1] Undergraduate Department, Indian Institute of Science (IISc), Bengaluru, India
[2] Materials Research Centre, Malaviya National Institute of Technology (MNIT), Jaipur, India
[3] Shodh Lab, Suresh Gyan Vihar University, Jaipur, India

their remarkable accuracy, low cost, sensitivity, and ease of use (Piovesan et al. 2020).

No expensive equipment or specialized skills are needed to use electrochemical sensor devices. For in-situ environmental pollution analysis, the instruments can be scaled. SPEs allow direct electrochemical processes to be carried out outside centralized laboratories (Renedo et al. 2007). SPEs have been praised as effective transducers for environmental testing because of their qualities, including mass manufacture, low power consumption, rapid response, and compactness (Couto et al. 2016). Therefore, just 50 µL of solution may be required for a SPE (Li et al. 2017). Like this, the working electrode area of the SPEs may be readily altered to increase sensitivities, decrease detection limits, and increase the selectivity of electrochemical techniques (Santana and Spinelli 2020).

Malathion is challenging to identify directly using electrochemical techniques since its redox pathways are not aided by a catalyst. Metal–organic frameworks (MOFs) are crystalline materials with a hierarchical porous structure. MOFs offer a broad spectrum of functions, including a strong absorption affinity and a large surface area (Easun et al. 2017). Yet, the electrical conductivity of these materials limits their electrochemical applications. Monometallic MOF transition metal ions improve the electrochemical characteristics of a MOF via induced lattice distortion, interfacial electron coupling, and combinatorial impact of metal ions. Furthermore, monometallic MOFs have extensive active areas and stability; therefore, they are well suited to electron transport catalytic processes. Co/Mn MOF for dichlorvos determination (Sankhla et al. 2024a), Mn/Fe MOF for chlorpyrifos determination (Janjani et al. 2022), and Cu/Ce MOF derivative for determination of malathion (Xie, et al. 2019) are the recent publications using MOFs for electrochemical sensing.

Many MOFs were used as electrochemical sensors to detect malathion, and the results were encouraging. Some examples of such materials are Cu-MOF (Al'Abri, et al. 2019), Cu/Co MOGs (He et al. 2023), and Ce(III, IV)-MOF (Ma et al. 2022). They exhibited high sensitivity, selectivity, and stability for efficient malathion detection. These findings show that MOF-based sensors can be used in monitoring the environment and public health, which constitutes a firm background for further studies on this topic. We discuss the importance of our paper in the literature, which emphasizes how MOFs can enhance the efficiency of electrochemical sensors for malathion detection.

A branch of MOFs is made up of luminescent metal–organic frameworks (LMOFs) (Ding et al. 2019; Liu et al. 2019). LMOFs have improved optical characteristics because of their ordered structure and adjustable pores (Yang et al. 2021), which gives them tremendous potential for advancement along with their usage in the field of luminescence sensing (Cai and Jiang. 2017; Wang et al. 2022). Amino acids, antibiotics, pH, small molecules, insecticides, anions, and cations (Sankhla et al. 2024b; Hu et al. 2022; Chen et al. 2022) are just a few of the targets these sensors have been used to investigate thus far. Much study has been focused on designing and developing MOF-based multi-functional sensors because MOFs demonstrate efficient and multi-functional detecting capabilities. Several reports of luminous MOFs have detected multiple targets (Wang 2023).

In recent advancements, Kim et al. (Kim et al. 2023) demonstrated the synthesis of electrospun manganese-based metal–organic frameworks (MOFs) for creating MnOx nanostructures embedded in carbon nanofibers, showcasing their potential as high-performance nonenzymatic glucose sensors. Their work highlights the versatility and effectiveness of Mn-MOFs in electrochemical sensing applications, emphasizing the integration of MOFs with conductive substrates to enhance sensor performance. In this study, we used Mn^{2+} metal centers in MOF frameworks to produce a monometallic Mn-MOF. The Mn(II) ion pairs exhibit high synergism due to their size, which improves electron transit. Incorporating metallic ions inside the framework enhances the quest for redox catalytic reactions, and subsequent malathion determination was achieved. The resulting structure has long-range disorder and high porosity. Because of this, incorrectly positioned metal coordination sites within the framework developed catalytic activity to absorb malathion and subsequent electro-reduction. Mn-MOF was used to improve the surface of screen-printed electrodes for the electrochemical determination of malathion. Mn-MOF was dispersed in an ethanol solution for the optical determination of malathion. So, we have used Mn-MOF for opto-electrochemical studies in this article.

Experimental

Reagents

Each chemical employed was unaltered and of analytical grade. Alfa Aesar, USA, provided a 5% w/w dispersion of NafionD-521 in water with 1-hydroxypropane, while Sigma-Aldrich, USA, provided malathion. Potassium ferricyanide, potassium ferrocyanide, N, N′-dimethylformamide, and terephthalic acid (H_2BDC) were supplied by Loba Chemie of India. Merck of the USA provided manganese chloride hexahydrate ($MnCl_2.4H_2O$) and ethanol.

Synthesis of monometallic Mn-MOF

As reported in the literature, a solvothermal technique was used to create monometallic MOF containing manganese ions (Qi et al. 2019). $MnCl_2.4H_2O$ has a total molar amount of 0.003 mol. MnCl2.4H_2O (0.003 mol, 0.593 g) was dissolved in 10 mL of ethyl alcohol solution, BDC (0.00075 mol, 0.125 g) was dissolved in another 10 mL of ethyl alcohol solution, and stirring was employed to speed up the dissolving process. After that, the solutes were continuously shaken and dropped into 10 mL DMF. DMF while being constantly agitated. Finally, the solution was transferred to a Teflon-linked autoclave (0.1 L) after a furious hour of stirring. For 12 h, the autoclave was heated to 150 °C in an oven. The sample was filtered and carefully cleaned with DMF and ethanol three times after it had cooled to room temperature. Before being collected, the material was dried in a vacuum oven for 12 h at 60 °C.

Characterization of Mn-MOF

With the use of a field emission transmission electron microscope (TEM-Titan Themis), we looked at the surface morphology of the produced MOF. The phase of MOF (X'Pert PRO, PANalytical, Netherlands) was characterized using an x-ray diffractometer with CuKα radiation, with a wavelength of 0.154 nm and a step size of 0.02° in two scan ranges of 4°–80°. Several functional groups of the artificially created MOF were evaluated using the attenuated total reflectance (ATR) configuration of Fourier transforms infrared (FT-IR) spectroscopy (Alpha, Bruker, Germany) within a wavenumber spanning from 500 to 4000 cm^{-1}. A Raman spectrometer (P785, Tracer) was utilized to acquire significant vibrational characteristics for the functional groups under Ar ion laser irradiation at 785 nm.

Fabrication of a sensor based on Mn-MOF

The sensor has an auxiliary, working, and reference electrode and was created using three-in-one screen-printed carbon electrodes that are available for purchase. Prior to modification, SPE underwent 10 scans at a rate of 0.1 V/s using 0.05 mL of a 0.5-M sulfuric acid solution as the electrolyte. The potential scan range was − 0.5 V to + 0.5 V. A pre-treatment method increased the SPE's functionality and surface roughness, which increased its voltamperometric responsiveness. De-ionized water was then used to clean the SPE.

The produced Mn-MOF was ultrasonically dispersed to a concentration of 1 g/mL in a 10:1 mixture of isopropyl alcohol and Nafion polymer solution in order to alter the electrode's surface. Dropcasting a 5-µL sample from the modified dispersion onto the SPE working electrode's base, the sample was allowed to dry and develop a uniform layer in the ambient environment. The modified electrode with Mn-MOF/SPE is also used in sensing applications.

Electrochemical measurements

A potentiostat (Sensit Smart) was utilized in each electrochemical study, and the experimental parameters were managed by PS Trace 5.9 software. An aqueous solution containing 0.1 M KCl and a 5-mM $[Fe(CN)_6]^{3-/4-}$ redox probe was used as the electrolyte for the electrochemical testing of Mn-MOF/SPE. Every test was carried out at room temperature. CV investigations were carried out at a scan rate of 0.1 V/s throughout a potential range that varied from − 1.2 V to 1 V. For electrochemical impedance spectroscopy (EIS) measurements, a DC voltage of 0 V against a reference and a pulse amplitude of 0.01 V was employed, spanning the frequency range of 1 Hz to 100 kHz.

Quantification of malathion

The surface-modified Mn MOF/SPE found malathion at various quantities ranging from 30 µL to 170 µL. In 0.1 M KCl aqueous medium solution with 5-mM $[Fe(CN)_6]^{3-/4-}$ redox probe, experiments for square wave voltammetry (SWV) were conducted. SWV was performed at a frequency of 10 Hz, an amplitude of 0.15 V, and a step height of 0.01 V in the potential range of − 1.0 V to 1.0 V. The importance of variables like elution duration was increased for effective malathion quantification. The behavior of the synthesized MOF's absorption was also studied. Additionally, the adsorption behavior of the synthesized MOF was examined using double potential step chronocoulometric (DPSC), where the forward and reverse potentials were, respectively, 0.5 V and − 0.5 V. (0.1 s pulse width).

Fluorescent sensing experiment

An RF-6000 fluorescence spectrophotometer was used to record the fluorescence spectra. LabSolutions RF version 1.17 was utilized to control the experimental conditions, and the parameters that were employed are EM wavelength end: 5800 Å, EM wavelength start: 2500 Å, EX wavelength: 2600 Å, data interval: 10 Å.

An hour was spent sonicating 2 mg of Mn-MOF that had been dissolved in ethanol for the fluorescence sensing experiment. The solution steadied into a suspension after a few while.

Results and discussion

Material characterizations

Figure 1a depicts the synthesized Mn-MOF's powder x-ray diffraction (PXRD) pattern. The detected peaks

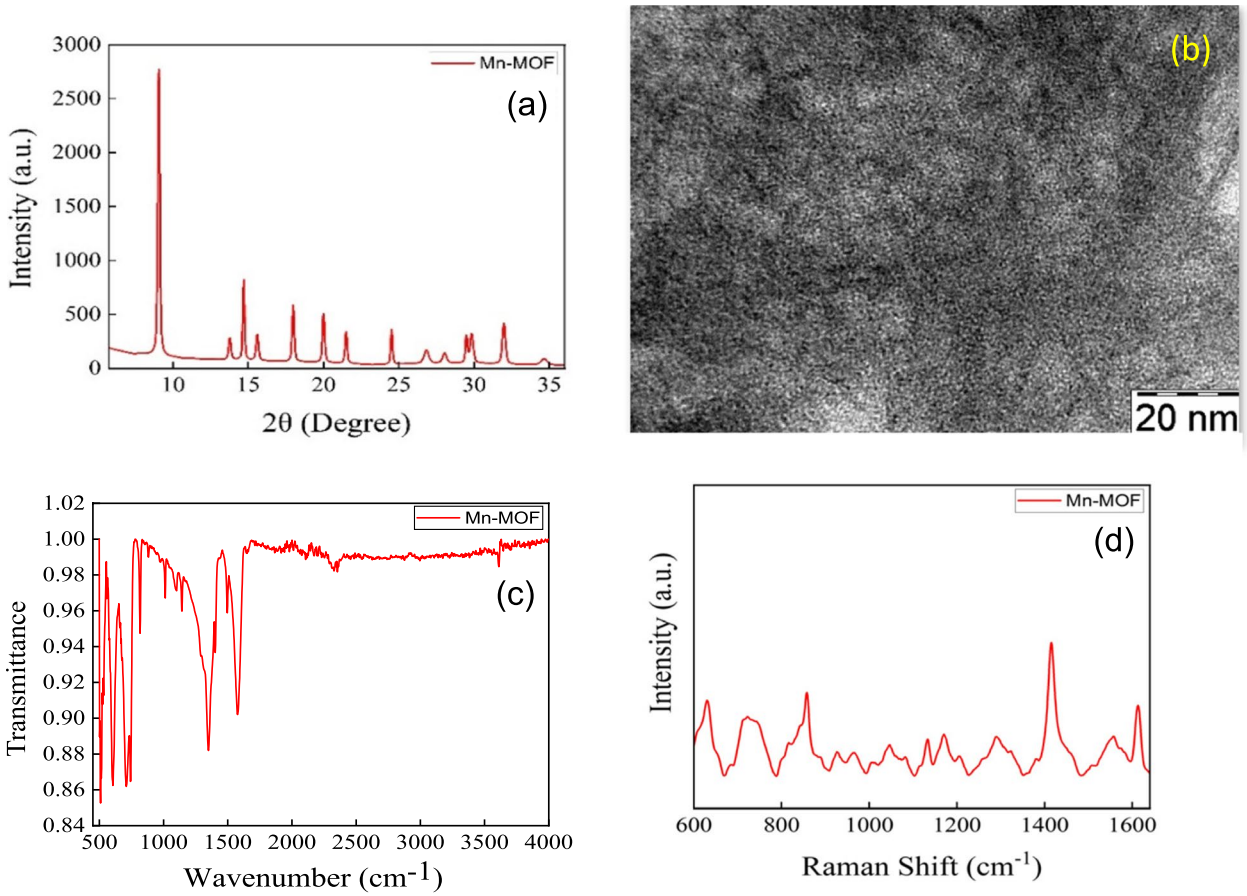

Fig. 1 **a** XRD of Mn-MOF. **b** TEM image of Mn-MOF. **c** FT-IR spectrum. **d** Raman spectrum

for Mn-MOF were 26.825°, 24.515°, 21.485°, 20.015°, 18.005°, 15.575°, 14.705°, 13.775°, and 9.065°. These values are almost identical to those reported in the previous study (Sundriyal et al. 2019). The average crystalline size was 12.38 nm, as determined by the Debye–Scherrer equation:

$$D = (0.9 \times \lambda)/(cos\theta \times \beta)$$

where θ, β, λ, and D represent Bragg's angle, full width at half maxima wavelength, x-ray, and crystalline size, respectively.

Figure 1b displays the surface morphology of the synthesized Mn-MOF analyzed by transmission electron microscopy. It has a homogeneous, flexible laminar structure. This refers to the previously mentioned article (Joshi et al. 2022). Because there are more active sites on the porous surface of Mn-MOF, a greater surface area is available for porosity and adsorption, which is advantageous in electroanalysis.

The FTIR spectra of the Mn-MOF are shown in Fig. 1c, demonstrating the presence of several additional functional groups. New bands are seen in Mn-MOF at 1391 cm^{-1}, which are attributed to symmetric stretching vibrations of –COO–, and 1564 cm^{-1}, which are attributed to asymmetric stretching vibrations of the same compound. These results demonstrated that after complexing with Mn ions, acidic COOH was deprotonated (Sundriyal et al. 2019).

As seen in Fig. 1d (Pabbi et al. 2018), vibrational modes were investigated using Raman spectroscopy. Peaks at 857 cm^{-1}, 720 cm^{-1}, and 632 cm^{-1} represent the C–H bonding of the synthesized Mn-MOF, whereas the aromatic ring bond for the C=C is seen at 1612 cm^{-1} (Joshi et al. 2022). About 1415 cm^{-1} is where carboxylate asymmetric vibration maxima were discovered (Janjani et al. 2022). According to our findings, H_2BDC coordinated with Mn(II) metal ions to form a stable structure.

Electrochemical examination

Figure 2a depicts the cyclic voltammograms acquired for Mn-MOF/SPE as well as bare SPE in 0.1 M KCl solution using a 5-mM $Fe(CN)_6^{3-/4-}$ redox probe at a 100-mV/s

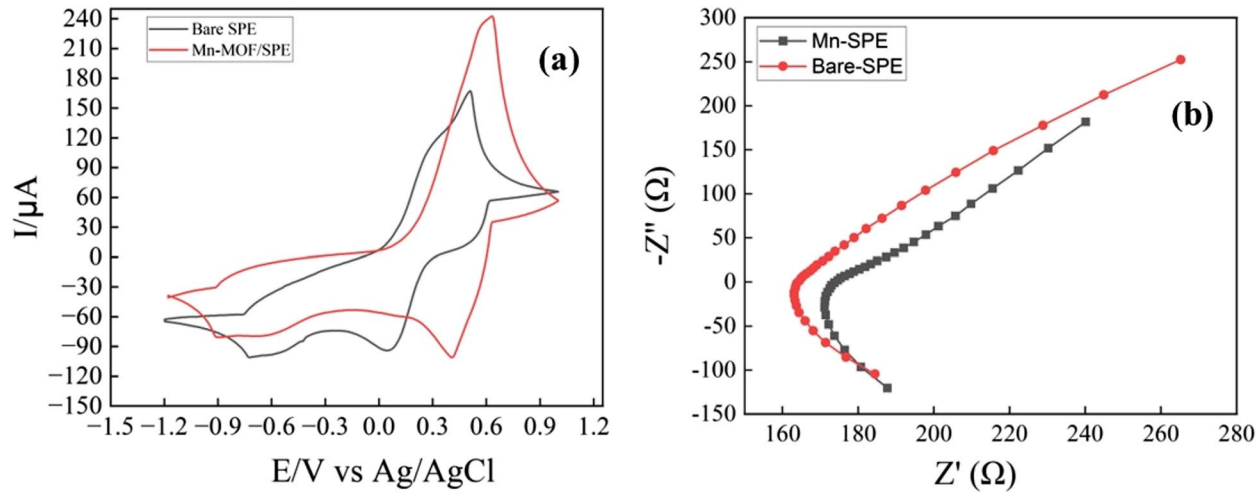

Fig. 2 **a** CV of Mn-MOF/SPE and bare SPE electrodes and **b** EIS Nyquist graphs of Mn-MOF/SPE and bare SPE electrodes (inset fitted Randle's circuit)

scan rate. For Mn-MOF/SPE and bare SPE, the potential value and anodic peak current remained at 0.637 V and 243.3μA and 0.515 V and 168.3μA, respectively. For Mn-MOF/SPE and bare SPE, the cathodic peak current and potential value remained − 101.1 μA and 0.413 V and − 93.86 μA and 0.055 V, respectively. 0.224 V and 0.46 V are the peak-to-peak separation potentials for Mn-MOF/SPE and bare SPE, respectively. Peak-to-peak separation decreases and, along with these, peak current increases for working electrodes treated with Mn-MOF/SPE, implying quicker electron transport after electrode alteration. The peculiar shape and synergistic effect induced by the metal ions in the Mn-MOF/SPE structure may be responsible for the better redox behavior of the Mn-MOF-modified SPE (Tang et al. 2022).

The Randles–Sevcik equation was used for the determination of electroactive surface area, which was derived as described in the following:

$$I = 2.687 \times 10^5 n^{3/2} A D^{1/2} C v^{1/2}$$

where concentration (mol cm^{-3}) is denoted by C, maximum current (Ampere) is denoted by I, the electroactive surface area (cm^2) is denoted by A, scan rate (Vs^{-1}) is denoted by v, the diffusion coefficient (7.2×10^{-6} cm^2 s^{-1}) is denoted by D, and during the redox process n is the number of electrons that are transferred (Pabbi et al. 2018). Figure S1 shows the cyclic voltammograms with both the original and altered electrodes. The electrode surface area of Mn-MOF/SPE was about double that of bare SPE. The monometallic Mn-MOF surface-modified electrode has a considerable increase in electrode surface area, which may boost the adsorption and coordination sites for malathion interactions.

Moreover, Mn-MOF/SPE demonstrated a reduced resistance to charge transfer (Rct) of 0.00072 mΩ compared to bare SPE at 0.001 mΩ. Rct arose because of electron charge transport restrictions between the electrolyte and the modified electrode. The fitted Randle's circuit and EIS spectra of these are shown in Fig. 2b. In its Nyquist plot, Mn-MOF had a narrower semicircle than bare SPE. The EIS and CV investigations validated the SPE surface alteration using monometallic Mn-MOF, demonstrating more electrocatalytic activity and charge transfer kinetics enhancement than bare SPE.

Electrochemical activity of Malathion upon Mn-MOF/SPE

The redox behavior for malathion upon Mn-MOF modified electrode has been examined by adjusting the potential scan rate of CV on a scale spanning 0.05 to 3 V/s in Fig. 3a. The peak current magnitude increases linearly with increments in scan rate, as seen in Fig. 3b. Figure S2 shows a correlation between the peak current and logarithms of the scan rate, demonstrated by the adsorption-regulated aspect of the electrode method (Shih et al. 2004).

Moreover, the regression equations reflect peak potential fluctuation for increasing scan rate, as illustrated in Fig. 3c:

$$E_{pa} = 0.129 \log v + 0.777$$
$$E_{pc} = -0.034 \log v - 0.893$$

The cathodic peak potential and the anodic peak potential are represented by E_{pc} and E_{pa}, respectively, and the scan rate is denoted by v. Laviron's theory (Laviron 1979) explains that these equation's slopes were equal to $-2.3RT/\alpha nF$ for cathodic peak and $2.3RT/(1-\alpha)nF$ for anodic peak. Here, n denotes the quantity of reacting

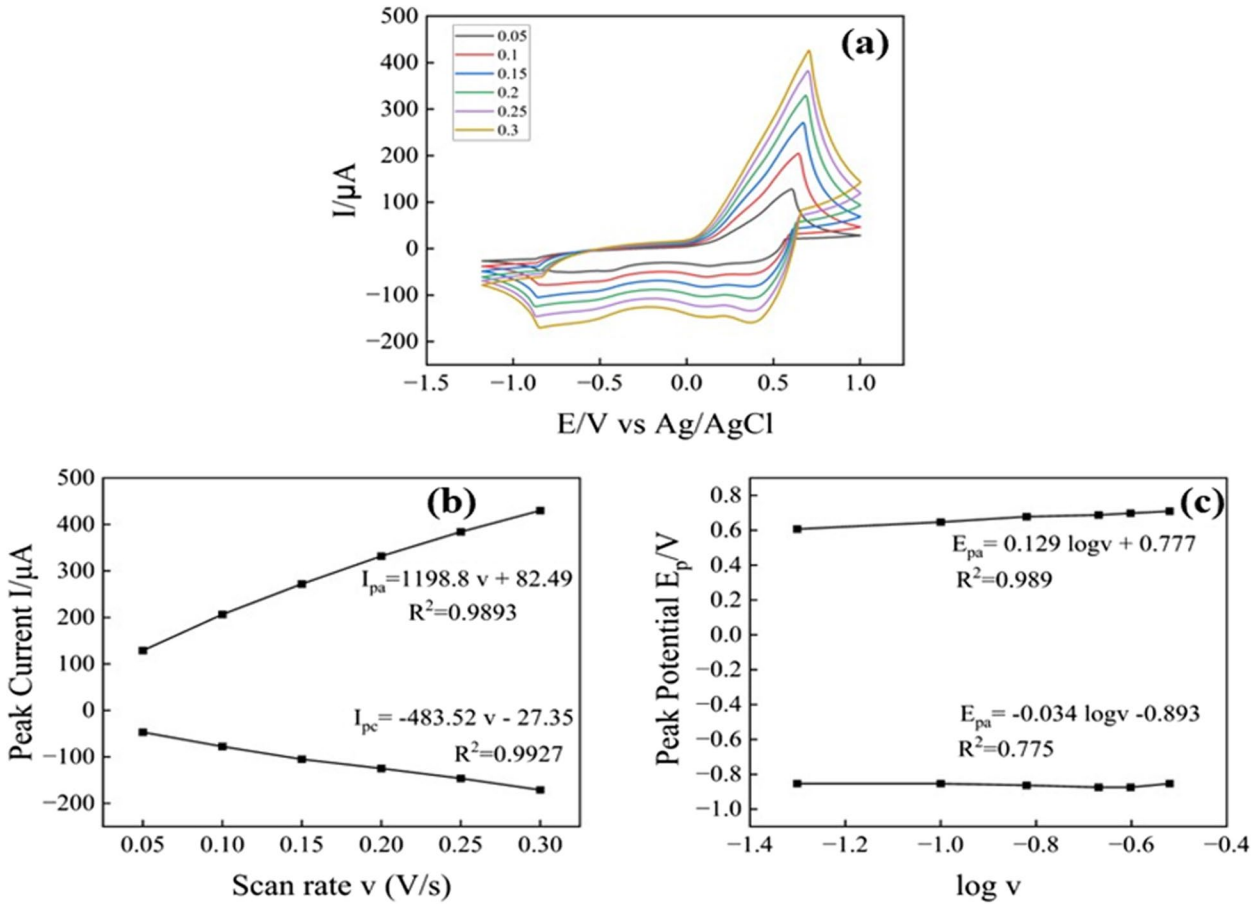

Fig. 3 **a** Cyclic voltammograms in 0.1 M KCl solution using a 5-mM $Fe(CN)6^{3-/4-}$ redox probe of 10 µM malathion on Mn-MOF/SPE with varying scan rates from 0.05 to 0.3 V/s. **b** Peak potential vs scan rate logarithm. **c** Peak current vs potential scan rates

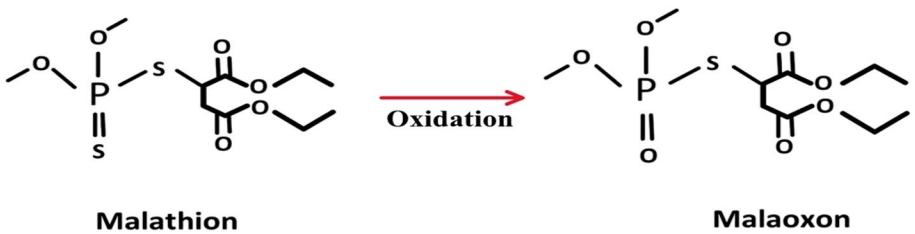

Fig. 4 The mechanism for malathion driven by Mn-MOF/SPE transducer

electrons, and α denotes the electron transfer coefficient. n and α were determined to be 2.2 and 0.79, respectively. Malathion, therefore, underwent a two-electron electrochemical reaction. As was already said, Fig. 4 shows a method for the mechanism of malathion (He et al. 2023).

Moreover, the organophosphate malathion, which was detected in 0.1 M KCl solution using a 5-mM $Fe(CN)_6^{3-/4-}$ redox probe, was used to assess the electrochemical adsorptive effectiveness of both the surface-modified and unmodified electrodes. The charge vs. $(time)^{1/2}$ graph of Mn-MOF/SPE and bare SPE, respectively, are shown in Fig. 5's Anson plots (Anson1 n.d.). The difference between the forward and backward step linear plot's y-axis intercept readings referred to as the adsorbed faradic charge (Qads), depicts the number of active species adsorbed onto the electrode surface by the Cottrell theory. The Q_{ads} have been determined to be 1.407 mC for Mn-MOF/SPE and 0.60 mC for bare SPE. (Xu et al. 2020). The monometallic Mn-MOF modified electrode's mesoporous surface and

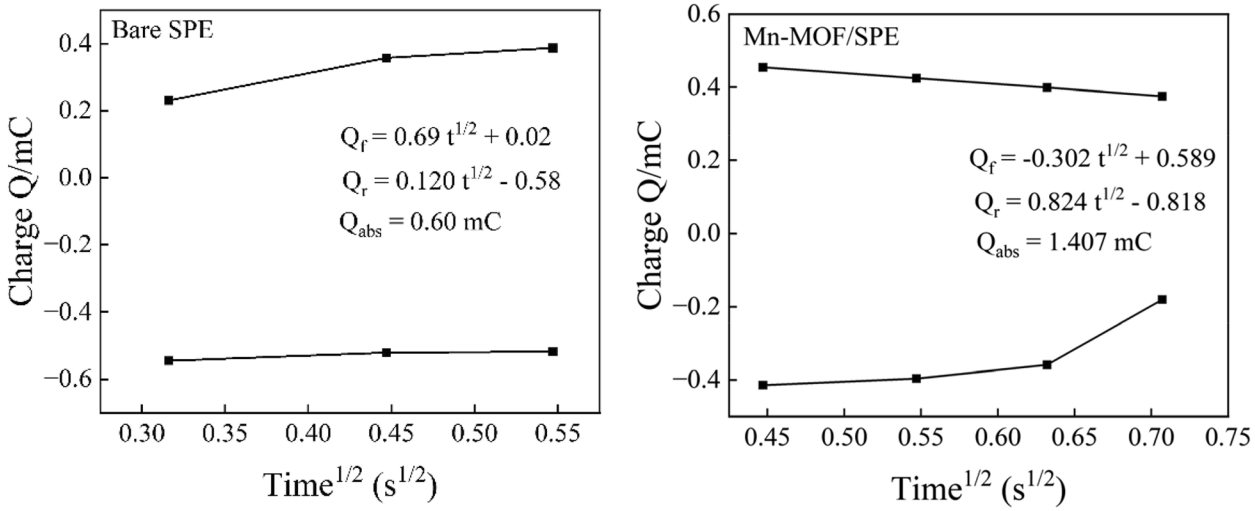

Fig. 5 *Q* vs. $t^{1/2}$ plotted during reverse and forward steps for Mn-MOF/SPE and Bare SPE

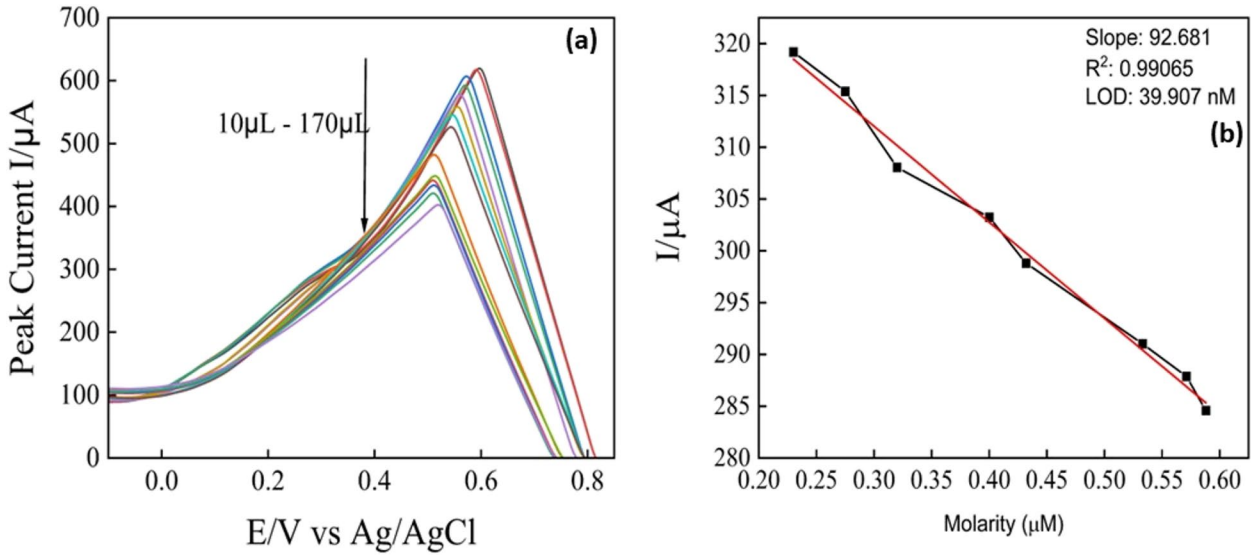

Fig. 6 **a** Malathion's SWV curves on Mn-MOF-SPE in the concentration range of 10 µL to 170 µl. **b** SWV analytic curve of malathion

remarkable electroactivity significantly enhance malathion adsorption.

Assessing Mn-MOF/SPE activity for malathion

The SWV approach was employed for sensing measurements because it improved discrimination for faradic currents. Figure 6a demonstrates the SWV responses for the Mn-MOF/SPE sensor at various malathion concentrations. A wide range of malathion concentrations were electro-analyzed to establish the electrochemical sensor's functioning range.

The peak current was shown to respond linearly to malathion concentrations between 10 and 170 µL with the regression equation $I_{SWV}(\mu A) = -92.68\ C(\mu M) + 339.824$ with correlation efficiency is 0.99065 where the SWV current response is denoted by I_{SWV} and malathion concentration is denoted by C as shown in Fig. 6b. When malathion's concentration increased, the Mn-MOF/SPE probe's peak current response decreased. The limit of detection was computed as 39.907 nM using the 3(SD)/(slope) criteria, wherein the standard deviation is denoted by SD and the Slope is of the calibration curve. Perhaps as a result, Mn-MOF-SPE, across a wide

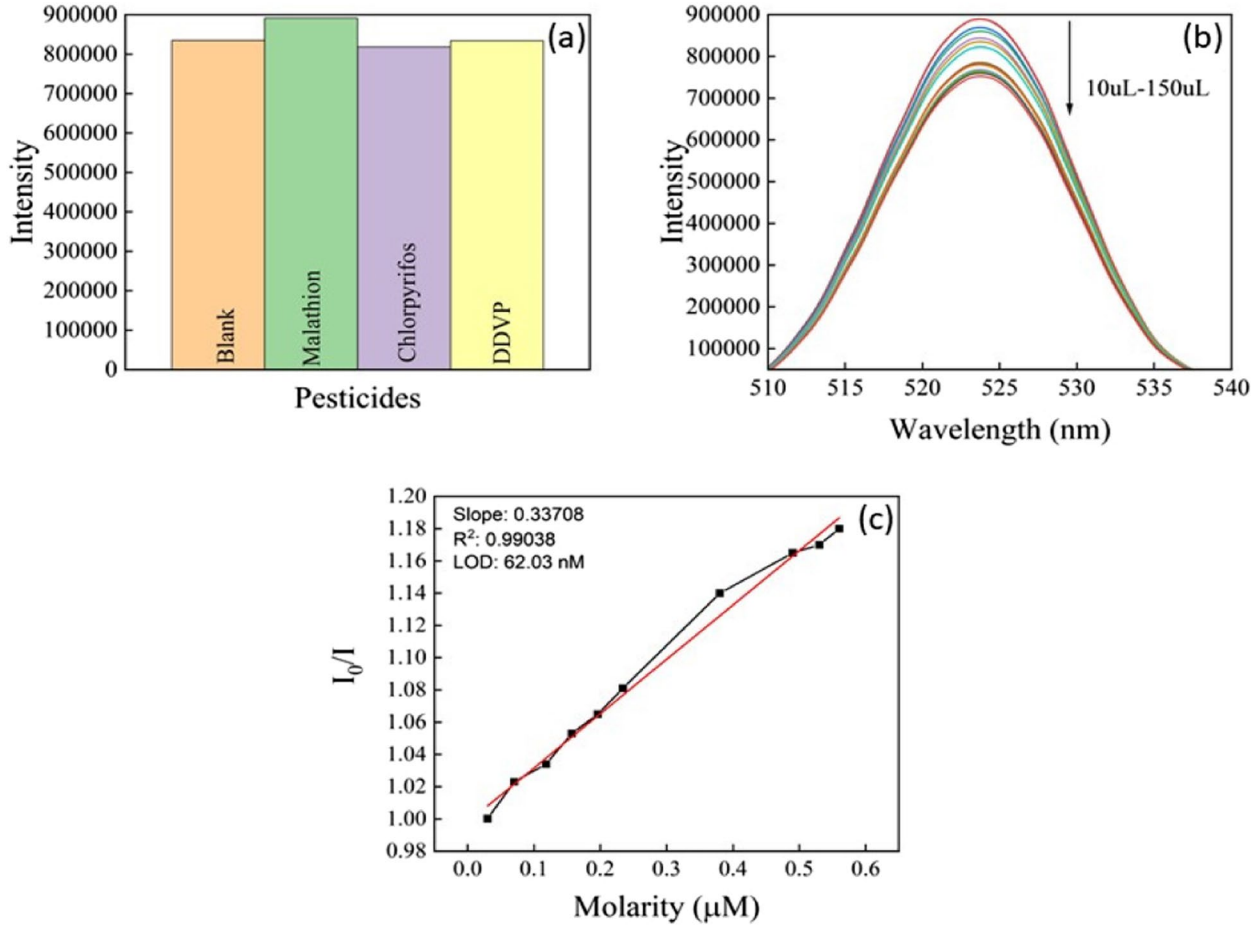

Fig. 7 **a** Fluorescence intensities of Mn-MOF in various pesticides. **b** Fluorescence spectra of Mn-MOF dispersed in different concentrations of malathion. **c** SV plot of Mn-MOF

concentration range, exhibited low detection limits and strong sensitivity for malathion.

Fluorescent sensing activity of Mn-MOF for malathion

An hour was spent sonicating 2 mg of Mn-MOF that had been dissolved in ethanol for the fluorescence sensing experiment. The solution steadied into a suspension after a few while.

Several pesticides were selected for fluorescence sensing, including DDVP, chlorpyrifos, and malathion. Figure 7a illustrates how applying the same amount of the other insecticides caused a variation in the fluorescence intensity. The remarkable selectivity of Mn-MOF was confirmed when the quenching rate of fluorescence intensity practically reached 99% with the addition of malathion.

To thoroughly study the fluorescence quenching behavior of Mn-MOF by malathion, concentration titration tests were conducted. Figure 7b displays the fluorescence spectra of Mn-MOF distributed in ethanol and different Malathion concentrations. Figure 7c illustrates the linear response of malathion concentrations to intensity in the range of 10 µL to 150 µL. As the concentration of malathion increased, the Mn-MOF's intensity response decreased. With a correlation efficiency of 0.99038, the detection limit was calculated as 62.03 nM using the 3(SD)/(slope) criterion, where SD and the slope indicate the calibration curve's standard deviation and slope, respectively. Consequently, Mn-MOF demonstrated excellent sensitivity to malathion and low detection limits over a broad concentration range.

Detection mechanism for optical sensing of malathion using Mn-MOF

Malathion detection using metal–organic frameworks (MOFs) involves several intricate mechanisms, each contributing to the fluorescence response changes observed during the sensing process. One primary mechanism is the photoelectron transfer (PET), where an excited electron transfers from the lowest unoccupied molecular

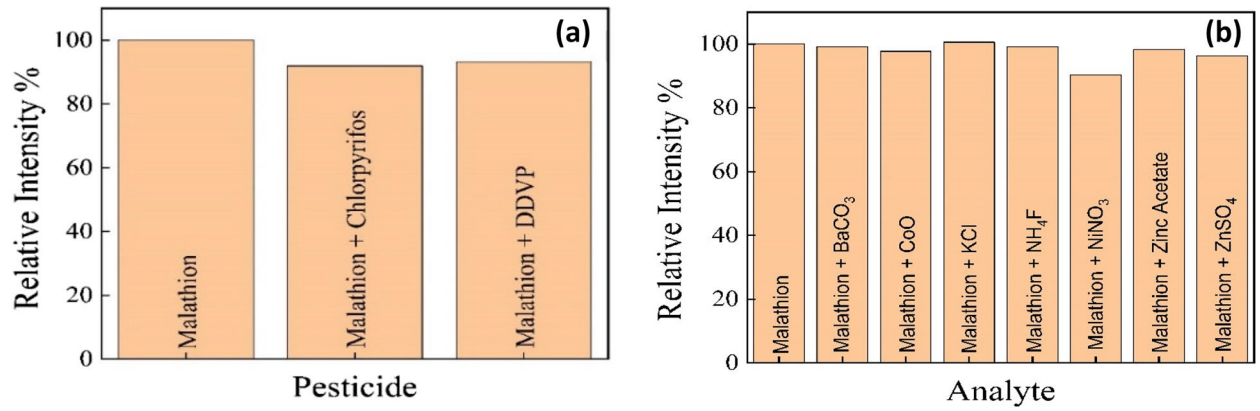

Fig. 8 **a**, **b** Malathion intensity response on a Mn-MOF mainly in different interferent chemicals

orbital (LUMO) of the photo-excited donor (MOF) to the LUMO of the acceptor (malathion). This electron transfer leads to fluorescence quenching, which is a crucial indicator in detecting the presence of malathion. The PET process largely depends on the energy levels of the donor and acceptor, which cause fluorescence quenching when the LUMO of MOF is at a higher energy level than that of malathion (Silva et al. 1997).

Forster resonance energy transfer (FRET) is another important mechanism in studying fluorescence. It is a non-radiative process whose efficiency changes depending on the distance between the donor (MOF) and acceptor (malathion), the extent of spectral overlap, and the dipole–dipole interaction between them. When malathion is present, it changes fluorescence in MOFs using FRET due to coinciding excitation and emission spectra. With this mechanism, susceptible detection can be provided for target analyte malathion since minor distance or spectral overlap variations may considerably affect the emitted light (Zhang et al. 2019).

The inner filter effect (IFE) is one of the most significant mechanisms for optical sensing with MOFs to detect malathion. This occurs through either adsorption of fluorescent emission onto the analyte (malathion) or competitive absorption of excitation light between the analyte and MOF. The IFE differs from PET and FRET because it does not depend on the distance between the MOF and malathion. Instead, this method relies on the overlap of the analyte's absorption spectrum with that of the MOF emission or absorption spectra, thus giving a way for visual fluorescence quenching in response to malathion detection (Sousaraei et al.. 2019).

Additionally, fluorescence features of MOFs can be affected by the presence of specific functional groups on the ligands; these are active sites for target recognition. Such groups change the fluorescence of MOFs via coordination or covalent interactions with them. During this detection process, malathion may interact with ligands or metal nodes in the MOF, leading to structural changes or even destruction of the MOF framework, causing changes in fluorescence intensity. Experiments conducted with Mn-MOFs and malathion have indicated that crystal structure and chemical links between units in the MOF stay unaltered during the sensing process, as suggested by Raman spectra, which is considerably consistent with literature S3. Nevertheless, quenching of fluorescence can also occur if an electron transfer occurs from fluorophore to malathion, as shown by Stern–Volmer curves (Fig. 7c), which exhibit linearity at low concentrations but divergence at higher values. These discoveries indicate a complex nature concerning fluorescence quenching and other factors like energy mismatch and absorption that influence optical sensing of malathion through using MOFs as platforms.

Table 1 Malathion content in real-world matrices

S. No	Analyte	Spiking concentration (μM)	Retrieved concentration (μM)	Retrieve (%)
1	Tap water	0.11	0.1186	100.5
2	RO water	0.079	0.102	129.35

Applicability of the Mn-MOF-based malathion optical sensor

Malathion's anti-interference effectiveness in the presence of other pesticides and ions was then studied. Other pesticides and ions did not interfere with malathion, as shown in Fig. 8a, b, and the maximal intensity change is a little less than 10%.

Table 2 Various papers were used to compare the electrochemical organophosphate determination

Nanoplatform	Technique	Organophosphate analyte	Dynamic range	Limit of detection	Reference
Mn-MOF-SPE	SWV	Malathion	0.89 µM and 5.95 µM	39.097 nM	Present work
COFTFPB-DBD/GCE	DPV	Malathion	10^{-12} g/L–10^{-8} g/L	3.0×10^{-13} g/L	Liang et al. 2021)
Ce(III, IV)-MOF	SWV	Malathion	1.0 µM~0.1 pM	0.045 pM	Ma 2022)
AChE/CS/Fe_3O_4	CV/Amperometry	Malathion	0.5 to 20 nmol L^{-1}	0.3 nmol L^{-1}	Rodrigues et al. 2018)
Mn-MOF	Fluorescence	Malathion	0.039 µM and 0.56 µM	62.03 nM	Present work
SiC@CuO-NPs	DPV	Malathion	0.03–3 nM	0.01 nM	Bakytkarim et al. May 2021)
CuO-NPs/3DGR/GCE	DPV	Malathion	0.03–1.5 nM	0.01 nM	Xie et al. Mar. 2018)
AChE/CNT-NH_2/GCE	DPV	Malathion	0.2–1 and 1–30 nM	0.08 nM	Yu et al. Jun. 2015)

The Mn-MOF sensor's analytical utility in the sample was tested using a spiked-recovery technique. Tap water and RO water were used as real sample matrices for electroanalysis, and the samples were spiked with malathion. Table 1 gives us the recovery percentage of malathion in tap water and RO water.

The experimental results show that Mn-MOF has a good selectivity for Malathion detection. Table 2 outlines the sensing performance of Mn-MOF with the performance of other reported electrochemical sensors for organophosphate.

As seen in Table 2, the innovative characteristics of the current work set it apart from previous studies. Using Mn-MOF as the sensing material is a novel strategy for determining organophosphate pesticides. High surface area, adjustable pore size, and outstanding stability are benefits of this metal–organic framework, all necessary for effective analyte detection. Using these characteristics, the sensor outperforms conventional sensing materials in terms of sensitivity towards malathion. Moreover, this sensor's use of a fluorescence quenching mechanism and electrochemical studies adds even more novelty. Although the opto-electrochemical technique is a well-known phenomenon, its use in malathion detection still needs to be explored, especially concerning MOF-based sensors. Through this technique, the sensor can reach a low detection limit, making it possible to detect malathion reliably at trace levels.

Among the other essential features of the sensor is the wide range of concentration it can cover. Some of the earlier works on detecting malathion have restricted their detection to either low or high concentrations of malathion. Still, the present work provides insightful material behavior toward malathion in the concentration range of 0.89–5.95 µM through square wave voltammetry (SWV). Fluorescence quenching was in the range of 0.039–0.56 µM. This wide action range guarantees that the sensor will be helpful where the presence of malathion at varying concentrations is possible. This is a unique and essential addition to the field of pesticide detection since the material used for sensing is Mn-MOF, the concentration range is significant, and opto-electrochemical techniques are used as an approach. This work sheds light on the MOF-based sensor and provides promising future research directions for designing high-performance detection platforms for detecting organophosphorus pesticides such as malathion.

Conclusion

This study presents the development of a non-enzymatic opto-electrochemical sensor for ultra-trace quantification of Malathion. The sensor is made from Mn-MOF, one of the monometallic MOFs that was scaled up in this research, and its properties were well characterized using different techniques like EIS, CV, FTIR, XRD, Raman spectroscopy, and TEM. These comprehensive investigations confirmed the solid cooperative interaction between the transition metal ions of the MOF framework and their high electrocatalytic activities toward Malathion with enhanced surface area. The newly developed sensor performed excellently by detecting Malathion at 39.907 nM by SWV technique and 62.03 nM by fluorescence quenching, as shown by SWV measurement and fluorometric analysis results. One significant benefit of this fabricated sensor was its exceptional selectivity towards common interfering chemicals, thus ensuring only reliable measurements. This sensor is highly robust for in-situ environmental pollution assessment and has simple assembly and installation. The present investigation provides an efficient and practical solution for tracking and examining minuscule levels of contamination with malathion in ecology through an Mn-MOF-based opto-electrochemical sensor. It can be used for other environmental monitoring purposes due to the low detection limit as well as excellent fluorescence response.

Supplementary Information

The online version contains supplementary material available at https://doi.org/10.1186/s40712-024-00157-9.

Additional file 1: Figure S1. Cyclic voltammograms of (a) Bare SPE and (b) Mn-MOF/SPE recorded at varying scan rates.The linear relationship between cathodic/anodic peak current and the square root of scan rate for Bare SPE and Mn-MOF/SPE electrodes, respectively. Figure S2. The linear relationship between anodic and cathodic peak current and logarithm scan rate. Voltammograms recorded in 0.1 M KCl solution using 5 Mm Fe63-/4- on Mn-MOF/SPE at scan rates. Figure S3. Raman spectra of Mn-MOF and the as-synthesized samples immersing in Malathion.

Acknowledgements
The authors thank the Water Technology Initiative (WTI) Program, Department of Science and Technology (DST), India (DST/TMD-EWO/WTI/2K19/EWFH/2019/222(C)) for funding the study. The authors would additionally like to acknowledge the Materials Research Centre, MNITJ, for providing the experimental and characterization equipment. The authors thank Ms. Manisha Gautam for her invaluable support during the project.

Authors' contributions
Lakshya Sankhla: Conceptualization, Methodology, Investigation, Formal analysis, Writing: original draft. Himmat Singh Kushwaha: Writing: review & editing, Supervision.

Availability of data and materials
All data generated or analyzed during this study are included in this manuscript. Further data related to this study can be available from the corresponding author upon reasonable request.

Declarations

Ethics approval and consent to participayte
Not applicable.

Competing interests
The authors declare that they have no competing interests.

Received: 6 April 2024 Accepted: 19 July 2024
Published online: 29 July 2024

References

Al'Abri AM et al (2019) Highly sensitive and selective determination of malathion in vegetable extracts by an electrochemical sensor based on Cu-metal organic framework. J Environ Sci Health Part B 54(12):930–941. https://doi.org/10.1080/03601234.2019.1652072
Anson1 FC n.d. Innovations in the Study of Adsorbed Reactants by Chronocoulometry Available: https://pubs.acs.org/sharingguidelines
Bakytkarim Y, Tursynbolat S, Huang J, Wang L (2021) Free-enzymatic Indirect Detection of Malathion by SiC@CuO-NPs Composite Nanomaterial Modified Glassy Carbon Electrode. ChemistrySelect 6(17):4056–4062. https://doi.org/10.1002/slct.202100904
Bonner MR et al (2007) Malathion exposure and the incidence of cancer in the agricultural health study. Am J Epidemiol 166(9):1023–1034. https://doi.org/10.1093/aje/kwm182
Cai G, Jiang HL (2017) A modulator-induced defect-formation strategy to hierarchically porous metal-organic frameworks with high stability. Angew Chem 129(2):578–582. https://doi.org/10.1002/ange.201610914
Chen FG et al (2022) Dysprosium(III) metal-organic framework demonstrating ratiometric luminescent detection of pH, Magnetism, and Proton Conduction. Inorg Chem 61(13):5388–5396. https://doi.org/10.1021/acs.inorgchem.2c00242
Couto RAS, Lima JLFC, Quinaz MB (2016) Recent developments, characteristics and potential applications of screen-printed electrodes in pharmaceutical and biological analysis. Talanta 146:801–814. https://doi.org/10.1016/j.talanta.2015.06.011. Elsevier B.V
de Silva AP et al (1997) Signaling recognition events with fluorescent sensors and switches. Chem Rev 97(5):1515–1566. https://doi.org/10.1021/cr960386p
Ding M, Flaig RW, Jiang HL, Yaghi OM (2019) Carbon capture and conversion using metal-organic frameworks and MOF-based materials. Chem Soc Rev 48(10):2783–2828. https://doi.org/10.1039/c8cs00829a. Royal Society of Chemistry
Easun TL, Moreau F, Yan Y, Yang S, Schröder M (2017) Structural and dynamic studies of substrate binding in porous metal-organic frameworks. Chem Soc Rev 46(1):239–274. https://doi.org/10.1039/c6cs00603e. Royal Society of Chemistry
He C, Yan R, Xue Q, Li S, Wang H (2023) Electrochemical malathion sensors based on phytic acid-doped polyaniline and overoxidized polyaniline nanorods. J Mater Sci. https://doi.org/10.1007/s10853-022-08052-4
He C, Yan R, Gao X, Xue Q, Wang H (2023) Non-enzymatic electrochemical malathion sensor based on bimetallic Cu-Co metal-organic gels modified glassy carbon electrode. Sens Actuators B Chem 385:133697. https://doi.org/10.1016/j.snb.2023.133697
Hu X, Zhang X, Cao H, and Huang Y (2022) Cu-based metal-organic frameworks-derived copper nanoclusters with tunable emission for ratiometric pH sensing. Sens Actuators B Chem 353 https://doi.org/10.1016/j.snb.2021.131130
Huang Y et al (2019) Determination of multi-pesticide residues in green tea with a modified QuEChERS protocol coupled to HPLC-MS/MS. Food Chem 275:255–264. https://doi.org/10.1016/j.foodchem.2018.09.094
Janjani P, Bhardwaj U, Gupta R and Singh Kushwaha H (2022) Bimetallic Mn/Fe MOF modified screen-printed electrodes for non-enzymatic electrochemical sensing of organophosphate. Anal Chim Acta 1202. https://doi.org/10.1016/j.aca.2022.339676
Joshi P et al (2022) Laser-patterned carbon coatings on flexible and optically transparent plastic substrates for advanced biomedical sensing and implant applications. J Mater Chem C Mater 10(8):2965–2975. https://doi.org/10.1039/d1tc05176h
Kim SE, Yoon JC, Tae H-J, Muthurasu A (2023) Electrospun manganese-based metal-organic frameworks for MnO_x nanostructures embedded in carbon nanofibers as a high-performance nonenzymatic glucose sensor. ACS Omega 8(45):42689–42698. https://doi.org/10.1021/acsomega.3c05459
Laviron E (1979) General expression of the linear potential sweep voltammogram in the case of diffusionless electrochemical systems Available: https://doi.org/10.1016/S0022-0728(79)80075-3. Accessed: 22 Oct 2022
Li M, Li DW, Xiu G, Long YT (2017) Applications of screen-printed electrodes in current environmental analysis. Cur Opin Electrochem 3(1):137–143. https://doi.org/10.1016/j.coelec.2017.08.016. Elsevier B.V
Liang H, Wang L, Yang Y, Song Y and Wang L (2021) A novel biosensor based on multienzyme microcapsules constructed from covalent-organic framework. Biosens Bioelectron 193 https://doi.org/10.1016/j.bios.2021.113553
Liu Y, Xie XY, Cheng C, Shao ZS, Wang HS (2019) Strategies to fabricate metal-organic framework (MOF)-based luminescent sensing platforms. J Mater Chem C 7(35):10743–10763. https://doi.org/10.1039/c9tc03208h. Royal Society of Chemistry
Ma D, et al (2022) Multiplexed electrochemical aptasensor based on mixed valence Ce(III, IV)-MOF for simultaneous determination of malathion and chlorpyrifos. Anal Chim Acta 1230, https://doi.org/10.1016/j.aca.2022.340364
Ma D et al (2022) Multiplexed electrochemical aptasensor based on mixed valence Ce(III, IV)-MOF for simultaneous determination of malathion and chlorpyrifos. Anal Chim Acta 1230:340364. https://doi.org/10.1016/j.aca.2022.340364
Malathion _ C10H19O6PS2 _ CID 4004 - PubChem n.d. Available: https://pubchem.ncbi.nlm.nih.gov/compound/Malathion#section=Depositor-Supplied-Synonyms
Pabbi M, Kaur A, Mittal SK, Jindal R (2018) A surface expressed alkaline phosphatase biosensor modified with flower shaped ZnO for the detection of chlorpyrifos. Sens Actuators B Chem 258:215–227. https://doi.org/10.1016/j.snb.2017.11.079

Piovesan JV, Santana ER and Spinelli A (2020) A carbon paste electrode improved with poly(ethylene glycol) for tannic acid surveillance in beer samples. Food Chem 326. https://doi.org/10.1016/j.foodchem.2020.127055

Qi X, Tian H, Dang X, Fan Y, Zhang Y, Zhao H (2019) A bimetallic Co/Mn metal-organic-framework with a synergistic catalytic effect as peroxidase for the colorimetric detection of H2O2. Anal Methods 11(8):1111–1124. https://doi.org/10.1039/c8ay02514b

Renedo OD, Alonso-Lomillo MA, Martínez MJA (2007) Recent developments in the field of screen-printed electrodes and their related applications. Talanta. 73(2):202–219. https://doi.org/10.1016/j.talanta.2007.03.050. Elsevier

Rodrigues NFM, Neto SY, Luz RCS, Damos FS and Yamanaka H (2018) Ultrasensitive determination of malathion using acetylcholinesterase immobilized on chitosan-functionalized magnetic iron nanoparticles. Biosensors (Basel) 8(1) https://doi.org/10.3390/bios8010016

Sankhla L, Abedeen MZ, Gupta R, Kushwaha HS (2024a) Screen-printed bimetallic cobalt-manganese metal-organic framework electrodes for electrochemical detection of dichlorvos. J Electrochem Soc 171(6):066505. https://doi.org/10.1149/1945-7111/ad51ac

Sankhla L, Patel R, Kushwaha HS (2024b) Development of an Optical Sensor for the Detection of 22-Dichloro Vinyl Dimethyl Phosphate (DDVP) Using Nickel–Benzene-14 dicarboxylic acid Metal–Organic Framework (Ni-BDC-MOF). ACS Sustainable Resource Management. https://doi.org/10.1021/acssusresmgt.4c00209

Santana ER and Spinelli A (2020) Electrode modified with graphene quantum dots supported in chitosan for electrochemical methods and non-linear deconvolution of spectra for spectrometric methods: approaches for simultaneous determination of triclosan and methylparaben. Microchimica Acta 187(4) https://doi.org/10.1007/s00604-020-04225-7

Shih Y, Zen JM, Kumar AS, Chen PY (2004) Flow injection analysis of zinc pyrithione in hair care products on a cobalt phthalocyanine modified screen-printed carbon electrode. Talanta 62(5):912–917. https://doi.org/10.1016/j.talanta.2003.10.039

Silva-Madera RJ et al (2021) Pesticide Contamination in Drinking and Surface Water in the Cienega, Jalisco, Mexico. Water Air Soil Pollut 232:2. https://doi.org/10.1007/s11270-021-04990-y

Sousaraei A et al (2019) Subppm amine detection via absorption and luminescence turn-on caused by ligand exchange in metal organic frameworks. Anal Chem 91(24):15853–15859. https://doi.org/10.1021/acs.analchem.9b04291

Sundriyal S, Mishra S, and Deep A (2019) Study of manganese-1,4-benzenedicarboxylate metal organic framework electrodes based solid state symmetrical supercapacitor. Energy Procedia, Elsevier Ltd 5817–5824. https://doi.org/10.1016/j.egypro.2019.01.546

Tang F et al (2022) Synergistic effect of Mn doping and hollow structure boosting Mn-CoP/Co2P nanotubes as efficient bifunctional electrocatalyst for overall water splitting. J Colloid Interface Sci 628:524–533. https://doi.org/10.1016/j.jcis.2022.08.037

Wang LB, et al (2023) Water-Stable Cd-MOF with fluorescent sensing of Tetracycline, Pyrimethanil, abamectin benzoate and construction of logic gate. Spectrochim Acta A Mol Biomol Spectros 285 https://doi.org/10.1016/j.saa.2022.121894

Wang N, Liu Z, Wen L, Zhang B, an Tao C and Wang J (2022) Aptamer-binding zirconium-based metal-organic framework composites prepared by two conjunction approaches with enhanced bio-sensing for detecting isocarbophos, Talanta 236 https://doi.org/10.1016/j.talanta.2021.122822

Xiao Z, Yang Y, Li Y, Fan X, Ding S (2013) Determination of neonicotinoid insecticides residues in eels using subcritical water extraction and ultra-performance liquid chromatography-tandem mass spectrometry. Anal Chim Acta 777:32–40. https://doi.org/10.1016/j.aca.2013.03.026

Xie Y et al (2018) CuO nanoparticles decorated 3D graphene nanocomposite as non-enzymatic electrochemical sensing platform for malathion detection. J Electroanal Chem 812:82–89. https://doi.org/10.1016/j.jelechem.2018.01.043

Xie Y, et al (2019) A CuO-CeO2 composite prepared by calcination of a bimetallic metal-organic framework for use in an enzyme-free electrochemical inhibition assay for malathion. Microchimica Acta 186(8) https://doi.org/10.1007/s00604-019-3684-2

Xu C, Liu L, Wu C and Wu K (2020) Unique 3D heterostructures assembled by quasi-2D Ni-MOF and CNTs for ultrasensitive electrochemical sensing of bisphenol A. Sens Actuators B Chem 310 https://doi.org/10.1016/j.snb.2020.127885

Yang GL, Jiang XL, Xu H and Zhao B (2021) Applications of MOFs as luminescent sensors for environmental pollutants. Small 17(22) https://doi.org/10.1002/smll.202005327 John Wiley and Sons Inc

Yu G, Wu W, Zhao Q, Wei X, Lu Q (2015) Efficient immobilization of acetylcholinesterase onto amino functionalized carbon nanotubes for the fabrication of high sensitive organophosphorus pesticides biosensors. Biosens Bioelectron 68:288–294. https://doi.org/10.1016/j.bios.2015.01.005

Zhang J, Zhou R, Tang D, Hou X, Wu P (2019) Optically-active nanocrystals for inner filter effect-based fluorescence sensing: Achieving better spectral overlap. TrAC, Trends Anal Chem 110:183–190. https://doi.org/10.1016/j.trac.2018.11.002

Publisher's Note